Verification, validation, and parameter study of a computational model for corrosion pit growth adopting the level-set method. Part I: Corrosion

A. Fayezioghani[a,*], R. Dekker[b], L. J. Sluys[a]

[a]*Computational Mechanics Group, Department of 3MD, Faculty of Civil Engineering and Geosciences, Delft University of Technology, Delft, The Netherlands*
[b]*Building Physics and Systems, TNO, Delft, The Netherlands*

Abstract

Corrosion is a phenomenon observed in structural components in corrosive environments such as pipelines, bridges, aircrafts, turbines, etc. The computational model of corrosion should enjoy two features: a) accurately considering the electrochemistry of corrosion and b) properly dealing with the moving interface between solid and electrolyte. There are several approaches to model corrosion such as using FEM with mesh refinement algorithms, combining FEM and level-set method, employing finite volume methods, adopting peridynamic formulation, and utilizing phase field models. Because of its accuracy, lower computational cost, and robust dealing with multiple pit merging, the model which combines FEM with level-set method is selected to be more extensively assessed in this paper. Part I focuses on demonstrating the model's capabilities of simulating pitting corrosion through a set of numerical examples which include numerical solution verification, experimental validation, and uncertainty quantification of model parameters and properties.

Keywords: Corrosion, finite element method, level-set method, moving boundary problem, validation, uncertainty quantification

1. Introduction

Corrosion is a material degrading phenomenon due to chemical or electrochemical reactions in structural components subjected to corrosive environments[1, 2, 3]. From a chemical point of view, corrosion of metals is the chemical reaction of metallic atoms with atoms in the environment. Examples of corrosion can be found in pipelines[4], aircrafts[5], turbines[6], bridges[7], etc.

Corrosion pit growth is challenging from a computational point of view because the moving interface between solid and electrolyte usually needs special computational modelling/treatment. The traditional treatment is done by the use of FEM with mesh refinement algorithms. This works well but it has two

---

drawbacks: a) its computational cost increases rapidly with the increase of irregularities during the pit development (e.g. when electrolyte reaches non-corroding grains or voids in the solid domain) and b) it needs special numerical techniques in case corrosion pits meet each other. The finite volume method can be used as another computational model to deal with the moving boundary problem [8]. However, because it does not explicitly model the interface between solid and electrolyte, it cannot automatically consider characteristics related to or phenomena extremely close to the interface. A third treatment is the use of a peridynamic formulation[9]. Peridynamics can be viewed as a formulation which implicitly defines a nonlocal behaviour of the interface in order to couple the kinetics of dissolution with the movement of the interface for pitting corrosion [10]. Although being a relatively new and trending computational treatment of the moving boundary problem, a peridynamic formulation requires costly considerations related to boundary conditions. Using a phase field model is another alternative [11]. In this model, a free energy functional specific for the problem has to be defined. Although it gives reasonable results, it is a highly computationally expensive model. The last model to discuss is the employment of FEM with the level-set method [12]. This model is similar to a phase field model but does not require to put effort in constructing the free energy functional and also can be decoupled from the dissolution problem in a one-way manner [13, 14, 15]. For a review of the mentioned models, the reader is referred to [16].

As briefly discussed above, using FEM with a level-set method does not lead to enormous computational costs because a) no change of FE mesh is needed and b) the level-set method can benefit from the time scale separation of boundary motion from the dissolution problem. Moreover, the level-set method is powerful in dealing with ionic flux irregularities and merging multiple corrosion pits [13]. More details of the properties of the model are discussed in the following sections. Part I focuses on more extensively demonstrating capabilities of the model proposed by Dekker et al. [15] in simulating pitting corrosion via a set of numerical example problems. First of all, sensitivity analyses of system response quantities (SRQs) of interest such as pit depth, pit width, and lacy cover to finite element mesh size and nonlinear solution time step size are performed for each example problem. If the SRQs are concluded to be insensitive to mesh and time step size, uncertainty quantification (UQ) of some model parameters (e.g. passivation concentration, saturation concentration, moving corrosion front concentration, etc.) or model properties (e.g. initial electrolyte domain size and boundary conditions, initial pit shape, etc.) or both is conducted. Numerical solution verification and experimental validation are also included in the example problems for which analytical solutions and experimental measurements are available, respectively. In addition, an example problem is designed to qualitatively show the capability of the model in merging multiple pits and dealing with non-dissolving solid inclusions.

2. Corrosion Kinetics

Consider a pit filled with electrolyte on the surface of a metal solid (see Figure 1). The metal atoms dissolve into the electrolyte according to the following chemical reaction

$$M \longrightarrow M^{z+} + z\, e^- \quad \text{on } \Gamma_I \tag{1}$$
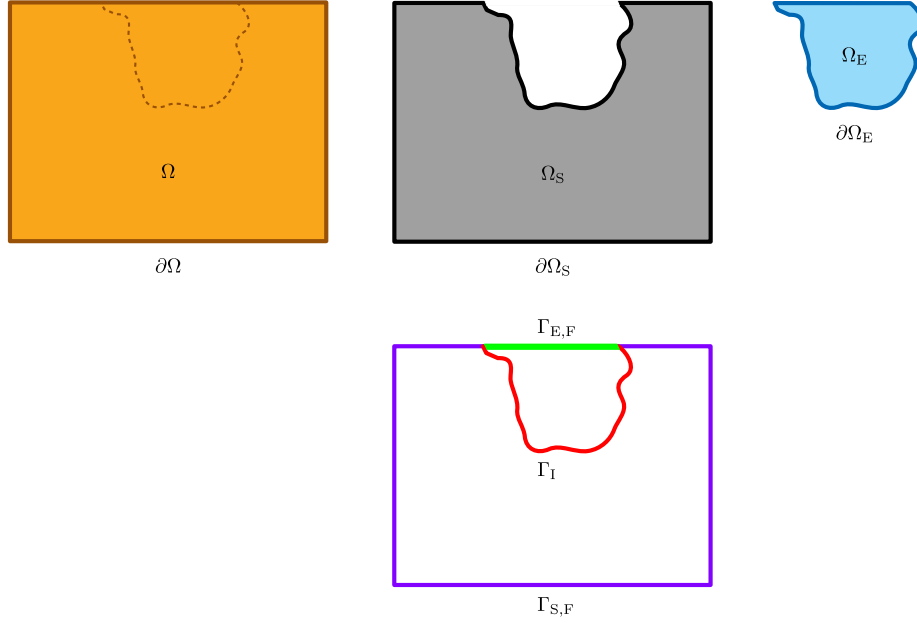
2

Figure 1: The domains of the problem and their boundaries in a two-dimensional space. Ω and $\partial\Omega$ illustrate the whole domain of the problem and its boundary, respectively. Ω_S and $\partial\Omega_\mathrm{S}$ illustrate the domain of the metal solid and its boundary, respectively. Ω_E and $\partial\Omega_\mathrm{E}$ illustrate the domain of the electrolyte and its boundary, respectively. As seen in the figure, the whole domain of problem $\Omega = \Omega_\mathrm{S} \cup \Omega_\mathrm{E}$, the interface between solid and electrolyte $\Gamma_\mathrm{I} = \Omega_\mathrm{S} \cap \Omega_\mathrm{E}$, the boundary of the whole domain of problem $\partial\Omega = (\partial\Omega_\mathrm{S} \cup \partial\Omega_\mathrm{E}) \backslash \Gamma_\mathrm{I}$, the non-overlapping boundary of solid with electrolyte $\Gamma_\mathrm{S,F} = \partial\Omega_\mathrm{S} \backslash \Gamma_\mathrm{I}$, and the non-overlapping boundary of electrolyte with solid $\Gamma_\mathrm{E,F} = \partial\Omega_\mathrm{E} \backslash \Gamma_\mathrm{I}$.

where M and M^{z+} indicate metal atom and metal ion, respectively, e^- is a symbol for an electron, and z is the valancy number of metal ion. Reaction (1) implies that the metal atom leaves the metal structure into the electrolyte giving z electrons. These electrons, here, are assumed to move toward a region in the metal away from the corrosion pit area so that they are not participating in the corrosion process anymore.

Since this paper and the employed model are based on microscale behaviour of stress corrosion, it is more practical to homogenize the distribution of metal ions in the electrolyte, to define a metal ion concentration (i.e. the amount of metal ions per unit volume), and to use it in the formulas instead of considering discrete metal ions. Therefore, according to the conservation of mass, mass transport of metal ions in the electrolyte is depicted by [17]

$$\frac{\partial c}{\partial t} + \nabla \cdot \boldsymbol{J} = 0 \quad \text{in } \Omega_\mathrm{E} \tag{2}$$

where c is metal ion concentration, t is time, $\partial/\partial\square$ is partial differential operator with respect to $\square$, $\nabla\cdot$ is the divergence operator, and $\boldsymbol{J}$ is molar flux of metal ions. According to the theory of dilute electrochemical solutions

$$\boldsymbol{J} = -D\nabla c \tag{3}$$

where D is the diffusion coefficient of metal ions. The following assumptions have been made in this contribution:

3

i) electric potential does not change from outside of corrosion pit towards corrosion front (i.e. the contribution of metal ion electromigration is neglected from equation (3))

ii) there is not any fluid flow in/out of pit area (i.e. the contribution of metal ion convection is neglected from equation (3))

iii) metal ions are not consumed/produced by chemical reactions in the pit area (i.e. sink/source of metal ions is neglected from equation (2))

Equations (2) and (3) result in a partial differential equation in which initial and boundary conditions are needed to be able to obtain a unique solution. The initial concentration of the metal ion c_{init} is usually assumed to be constant and uniformly distributed in the pit. Regarding boundary condition of the free surface of the pit (i.e. the surface of the electrolyte in the pit in common with the electrolyte outside of the pit), the metal ion concentration is usually assumed for this surface. The boundary condition of the interface between pit electrolyte and metal solid can be formalized for three possible conditions of metal ion concentration at each point: passivation, diffusion, and activation control condition [18]. Firstly, the passivation control condition means that there is no metal ion molar flux normal to the interface when the metal ion concentration is below a lower threshold:

$$\boldsymbol{J} \cdot \boldsymbol{n} = 0 \quad \text{on } \Gamma_{\text{I}} \text{ for } c \leq c_{\text{pas}} \tag{4}$$

where c_{pas} is the lower concentration threshold called passivation concentration and $\boldsymbol{n}$ is the unit outward normal vector to the interface, and $\cdot$ is the vector dot product. Because of the chemical reactions of chloride with metal ions, there will be an upper concentration threshold c_{sat}, called saturation concentration. Secondly, the diffusion control condition yields a saturation concentration at the interface points with concentrations close to saturation concentration:

$$c = c_{\text{sat}} \quad \text{on } \Gamma_{\text{I}} \text{ for } c \text{ close to } c_{\text{sat}} \tag{5}$$

Thirdly, the activation control condition takes place if the normal metal ion molar flux is directly dependent on the normal surface electric current density at the interface. In this case, the metal ion concentration is between the mentioned lower and upper thresholds. In activation control, according to Faraday's law of electrolysis [17]:

$$\boldsymbol{v}_{\text{f}} \cdot \boldsymbol{n} = \frac{j_{\text{n}}}{F z c_{\text{S}}} \quad \text{on } \Gamma_{\text{I}} \text{ for } c_{\text{pas}} < c < c_{\text{sat}} \tag{6}$$

where $\boldsymbol{v}_{\text{f}}$ is the velocity of the interface that is moving due to corrosion, j_{n} is normal surface electric current density, F is the Faraday constant, and c_{S} is the concentration of metal solid.

To summarize, equations (4), (5), and (6) are defined as the boundary conditions of the interface between metal solid and electrolyte for passivation, diffusion, and activation control conditions, respectively.

The interface is defined in a space which is one dimension lower than the solid and the electrolyte domains. For example, in a 3-, 2-, and 1-dimensional problem domain space, the interface is a surface, a curve, and a point, respectively. On the other hand, the concentration, as described earlier, is defined as
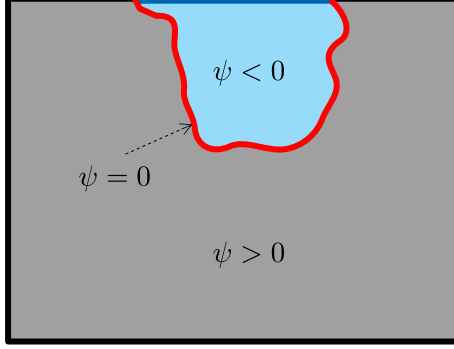
Figure 2: The regions divided by the level-set function: $\psi < 0$ in $\Omega_\text{E}\backslash\Gamma_\text{I}$, $\psi > 0$ in $\Omega_\text{S}\backslash\Gamma_\text{I}$, and $\psi = 0$ on Γ_I.

the amount of material per unit volume in the spatial space. Therefore, formulating the problem in terms of metal ion concentration involves a concentration jump through the interface. Consequently, the relation between velocity of the interface and normal metal ion molar flux is defined as

$$\boldsymbol{J} \cdot \boldsymbol{n} = -(c_\text{S} - c)\boldsymbol{v}_\text{f} \cdot \boldsymbol{n} \qquad \text{on } \Gamma_\text{I} \tag{7}$$

75 where $c_\text{S} - c$ is the concentration jump. The negative sign in the right hand side of equation (7) expresses that velocity of the interface and dissolution of metal mass occurring at the interface have opposite directions. It is worth noting that, in equations (4), (6), and (7), the spatial gradient of electric potential (and consequently electric current) is assumed to be zero except across the interface. 80 In other words, it is assumed that the electric current only occurs by dissolution of solid at the interface and normal to it.

3. Level-set method

In the previous section, the kinetics of dissolution of metal and mass transport in the electrolyte domain are provided. This section describes the motion 85 of the interface between metal and electrolyte and its computational modelling by the level-set method.

A scalar function ψ, called 'level-set', is assumed. The level-set function is negative in the electrolyte domain, positive in the solid domain, and zero at the interface between electrolyte and solid (see Figure 2). The evolution of ψ can be given as [12]

$$\frac{\partial \psi}{\partial t} + \boldsymbol{v}_\text{LS} \cdot \nabla \psi = 0 \qquad \text{in } \Omega \tag{8}$$

where $\boldsymbol{v}_\text{LS}$ is the level-set velocity vector field and ∇ is the gradient operator. Another form of equation (8) is obtained by substituting the more geometric equivalence of the dot product

$$\frac{\partial \psi}{\partial t} + v_\text{n}\|\nabla \psi\| = 0 \qquad \text{in } \Omega \tag{9}$$

where v_n is normal level-set velocity scalar field and $\|\square\|$ is the Euclidean norm of $\square$. Equation 9 will be simpler to solve if the level-set function satisfies the

5

signed distance characteristic:

$$\|\nabla\psi\| = 1 \quad \text{in } \Omega \tag{10}$$

Substituting (10) into (9) gives

$$\frac{\partial\psi}{\partial t} + v_{\text{n}} = 0 \quad \text{in } \Omega \tag{11}$$

Thus, instead of solving (9), one needs to firstly solve (10) and then update the level-set function by (11).

Since the motion of the interface (i.e. the evolution of the implicit surface $\psi = 0$) is of our interest, it is apparent to assume that the level-set velocity field normal to the interface should be equal to the normal velocity of the interface

$$v_{\text{n}} = \boldsymbol{v}_{\text{f}} \cdot \boldsymbol{n} \quad \text{on } \Gamma_{\text{I}} \tag{12}$$

However, an extension of the normal level-set velocity field is needed to the rest of the problem domain by [19]:

$$\nabla v_{\text{n}} \cdot \nabla\psi = 0 \quad \text{in } \Omega \tag{13}$$

The finite element method details of the numerical solution procedure of the corrosion problem together with level-set method are explained in [15].

4. Time scale separation of the moving boundary problem from the dissolution problem

The time scale of interface motion is much larger than the dissolution of metal ions into the electrolyte [20]. Thus, when combining FEM with the level-set method, it is possible to use separation of time scales in order to lower the computational complexity and cost. By benefiting from the time scale separation, we assume that the rate of change of boundary has negligible influence on the dissolution problem within the time scale of the dissolution problem. The following multiscale approach[21] is adopted to model the moving boundary problem in step i of an incremental numerical solution procedure:

1. The time interval, Δt_i, is selected to fall much below the time scale of the moving boundary problem.
2. The dissolution problem is solved assuming that the interface is stationary, $\text{d}(\Gamma_{\text{I},i})/\text{d}t = 0$, in the time interval Δt_i.
3. The rate of change of the interface, $\text{d}(\Gamma_{\text{I},i})/\text{d}t$, is calculated according to the solution of dissolution problem which is previously calculated.
4. The interface is evolved from $\Gamma_{\text{I},i}$ to $\Gamma_{\text{I},i+1}$ based on $\text{d}(\Gamma_{\text{I},i})/\text{d}t$.

5. Numerical examples

This section is designated for verification, validation, and uncertainty quantification of the corrosion model explained in previous sections. By 'verification', we mean checking numerical model against mathematical model; 'validation' is used to imply checking conceptual, mathematical, and numerical model against experimental data; and, 'uncertainty quantification' is a term which means that

6

Table 1: Model parameters used in the pencil test

F	=	$96485.3\,\mathrm{C\cdot mol^{-1}}$	c_{sat}	=	$5.1\times10^{-6}\,\mathrm{mol\cdot mm^{-3}}$
R	=	$8.314\,\mathrm{J\cdot mol^{-1}\cdot K^{-1}}$	c_{init}	=	$0.0\,\mathrm{mol\cdot mm^{-3}}$
z	=	2.19	D	=	$0.85\times10^{-3}\,\mathrm{mm^2\cdot s^{-1}}$
c_{S}	=	$143.0\times10^{-6}\,\mathrm{mol\cdot mm^{-3}}$	T	=	$288.15\,\mathrm{K}$
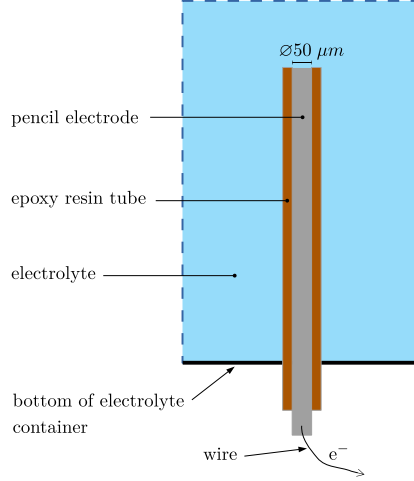
Figure 3: The pencil test set-up schematic view (adapted from [24]). The specimen is a cylindrical pencil electrode with 50 μm diameter which is covered by an epoxy resin tube. The electrons on the right hand side of corrosion reaction (1) leave the specimen via the wire at the bottom of specimen.

we are considering and quantifying different types of uncertainties (aleatory[1] and epistemic[2]) in the whole model [22]. Parameters of the model are listed in Table 1. If other values of these parameters are used or if determination of other parameters is required, they are explicitly mentioned in the text related to each example problem.

5.1. Example 1— Pencil test

This numerical example is a dissolution test of a steel electrode in an aqueous NaCl solution that is inspired from the experiments done by Ernst and Newman[23]. Figure 3 shows a schematic view of the test set-up and the dimensions of the specimen. The pencil electrode is covered by an epoxy resin so that dissolution occurs only in the cross sectional area of one end of the electrode. The other end of the electrode is connected to a wire in order to conduct the electric current away from the corrosion interface and to measure the electric current. Moreover, an electric potential of 600 mV versus SCE[3] is applied to the specimen to make sure that the corrosion pit quickly goes to diffusion control condition and consequently grows in a stable manner (i.e. without passivation).

---

[1]Uncertainty due to inherent randomness
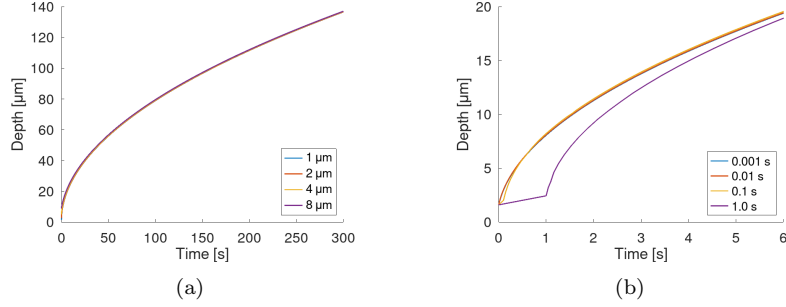[2]Uncertainty due to lack of knowledge
[3]Saturated Calomel Electrode

Figure 4: Mesh and time step size sensitivity of the depth evolution in the pencil test. (a) The depth of specimen in time shows negligible sensitivity to the simulated mesh sizes. (b) The depth obtained from all time step sizes rapidly approach to each other in a few seconds from start of the test.

The test is modelled in a two-dimensional space with 3-noded isoparametric triangular finite elements. The interface is assumed to be in diffusion control condition (i.e. the boundary condition (5)) during the entire simulation. In simulation cases where the top of the computational specimen is set as $\Gamma_{E,F}$ having the Dirichlet-type boundary condition (14) (see Figure 6(a)), the initial depth is set to a few micrometers. The reason is that it is not possible to define both the boundary condition of the interface and the electrolyte domain at the same time and location.

$$c = c_D \qquad \text{on } \Gamma_{E,F} \tag{14}$$

where c_D is a prescribed concentration. The depth of the pencil electrode in time is the system response quantity (SRQ) of interest in this numerical example.

Mesh and time step size sensitivity analyses of the model are done for the problem with boundary condition (14) where $c_D = 0$. Figure 4(a) shows depth of the specimen in time for time step size $\delta_{\text{time-step}} = 0.1$ s and four mesh sizes $\delta_{\text{mesh}} \in \{1.0, 2.0, 4.0, 8.0\}\,\mu$m. The figure shows almost identical results due to the linearity of the mass transfer equation (i.e. equations (2) and (3)) together with the diffusion control condition (5). In addition, the corrosion depth, again, shows only small differences between different time step sizes except in the very first times from start of the test. To more clearly observing this time step size sensitivity, Figure 4(b) illustrates the corrosion depth in a short time interval from the start of the test for $\delta_{\text{mesh}} = 1.0\,\mu$m and four time step sizes $\delta_{\text{time-step}} \in \{0.001, 0.01, 0.1, 1.0\}$ s. It is evident from Figure 4(b) that using a larger time step size gives a smaller depth. The reason for this minor step size dependence is the time scale separation assumed and discussed in Section 4, which causes underestimation of corrosion depth in case of diffusion control. However, the depths obtained from different time step sizes rapidly approach to each other in a few seconds so that one can neglect time step size sensitivity.

The depth obtained from the model is verified against an analytical solution of a one-dimensional diffusion controlled problem provided in [24]. Figure 5 shows the depth in time of the numerical analysis for $\delta_{\text{mesh}} = 1.0\,\mu$m and $\delta_{\text{time-step}} = 0.1$ s.

The depth obtained from the two-dimensional model utilized in this paper and the one-dimensional analytical solution coincide well to each other because
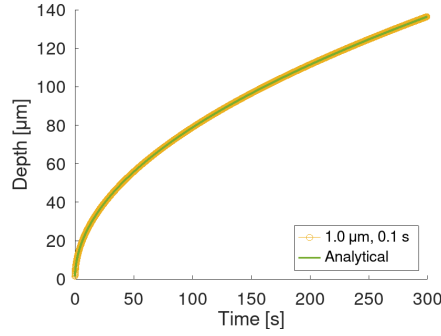
8

Figure 5: The model predicts the depth in time reasonably well in comparison to a one-dimensional analytical solution of a diffusion controlled problem.
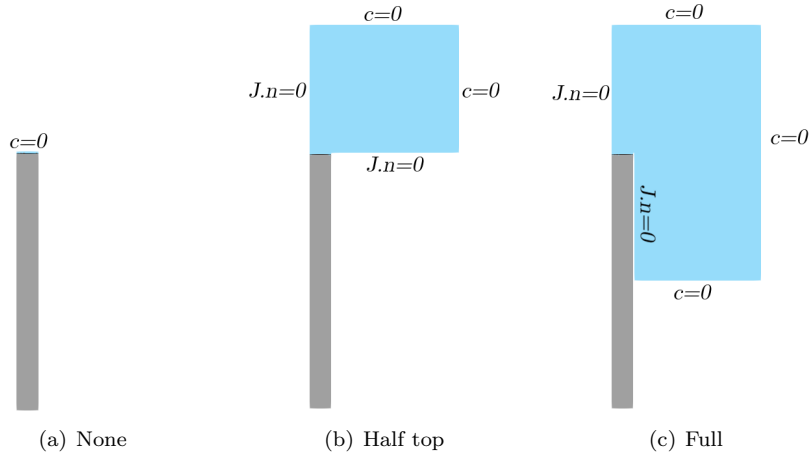

Figure 6: Different initial sizes and boundary conditions of the electrolyte domain. (Because of symmetry of the problem, only the right half of the specimen is illustrated.)

every metallic material point on the interface has the same condition and follows a one-dimensional vertical line to the free electrolyte surface when assuming the boundary condition given in equation (5). However, the real test cannot be assumed as a one-dimensional problem when considering a larger initial electrolyte domain above the pencil electrode. Thus, there is uncertainty in the sizes and boundary conditions of the initial electrolyte domain for the pencil test which is quantified here. See Figure 6 for different sizes and boundary conditions of the initial electrolyte domain. 'None' is defined as the condition in which metal ions immediately (almost) disappear out of the pencil test tube. Thus, no initial electrolyte domain is needed and the only boundary condition is a zero concentration at the top of the pencil test tube. In a computational (or an experimental) test with a thick noncorrodible and impermeable epoxy resin (compared to the pencil electrode diameter) around the pencil electrode, the 'Half top' condition is considered. The 'Full' condition is used in case a narrow noncorrodible and impermeable material covers the pencil electrode. The map of metal ion concentration at different times is illustrated in Figure 7 for

9

the three cases. Moreover, Figure 8 shows the depth evolution in time. As expected, the 'None' condition gives the deepest evolution of the interface among the different conditions; then, 'Full' shows less movement of the interface; and, finally, 'Half top' gives the smallest depth. The reason for these computational observations is that a non-zero metal ion concentration at the top of the pencil test tube in the 'Full' condition acts as an inherent barrier of metal ion mass transfer to leave the tube in comparison to the 'None' condition. This is also true for 'Half top' plus the fact that it restricts mass transfer more than 'Full' by considering an noncorrodible and impermeable surface at the bottom of the initial electrolyte domain outside of the pencil test tube. Moreover, the inherent ionic mass transfer barrier of the 'Full' and the 'Half top' condition are less restrictive for the interface points closer to the tube wall. This is because there are larger concentration gradients in horizontal direction for these interface points (see the slanted interface in Figure 7(a)). However, as the interface evolves and goes into the tube, the differences between the horizontal gradients of the interface points become smaller (see the interface position in Figures 7(b) and 7(c)). Therefore, it could be concluded that the easier the metal ion concentration is able to leave from the surface of the interface, the faster the interface moves. This conclusion gives support to the assumption regarding mass transfer with the diffusion controlled condition provided in Section 2.

The results of depth versus time of the simulations are presented together with the experimental measurement reported in [25] for stainless steel '304 SS' in 1 M NaCl at 15 °C in Figure 9. It is seen from the figure that the experimental measurement falls between the 'None' and the 'Full' conditions. That is, the metal ions in a short interval after the start of the test are transferred to the outside of the pencil test tube more easily than the 'Full' and more difficult than the 'None' condition. The reason of this observation might be the influence of the electric potential field inside the pencil test tube at early stages of the dissolution. This influence cannot be validated because a) the reported experimental data start from an almost linear part of the curve (around 25 s) and b) the model does not consider the electric potential field. Although there are differences in the predicted depths by the model in comparison to the experimental data, their slopes in Figure 9 become the same as time proceeds. This means that there is a transition time interval from the start of the test which simply causes a shift of depth afterwards.

## 5.2. Example 2— Two-dimensional pit test

This example, like the previous one, is designed to simulate the dissolution of metal into an aqueous NaCl solution in a two-dimensional corrosion pit (see Figure 10 for an schematic illustration of the specimen). All properties of the model are assumed to be constant through the thickness of the specimen. Furthermore, a constant applied surface electric current density of 15 mA/mm^2 is used in all simulations. Thus, a hybrid control scheme is adopted in this example. The hybrid control scheme initially assumes the activation control condition (6) over the entire interface and switches to the diffusion control condition (5) whenever the metal ion concentration of each point of the interface approaches the saturation concentration. It should be noted that the applied surface electric current density does not influence dissolution in diffusion control condition. In addition, the passivation condition (4) is not considered in this example. SRQs of interest are chosen to be maximum corrosion pit depth and

(a) $t = 20$ s

(b) $t = 100$ s

(c) $t = 300$ s

Concentration [mol\mm3]

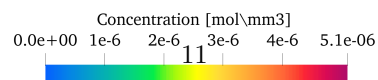0.0e+00   1e-6   2e-6   3e-6   4e-6   5.1e-06

11
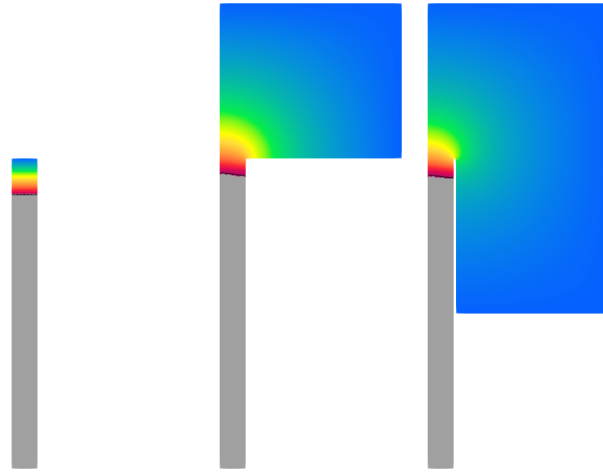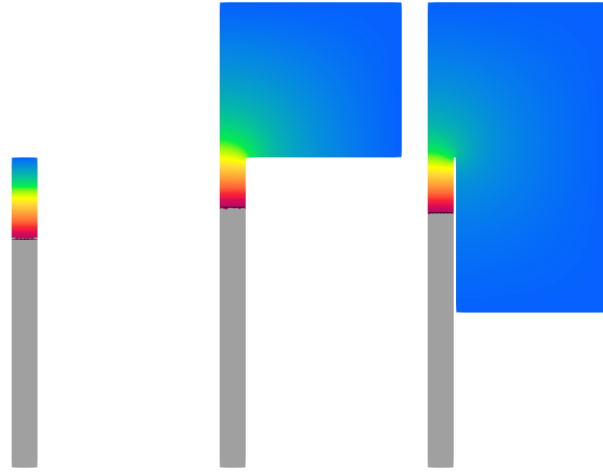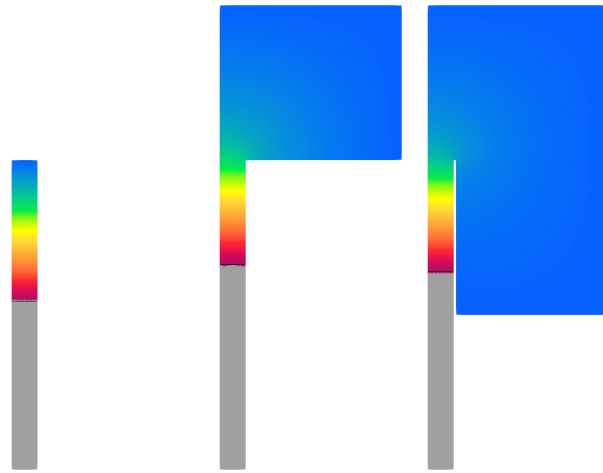
Figure 7: The map of metal ion concentration for different initial electrolyte size and boundary conditions (left to right: 'None', 'Half top', and 'Full') at $t = 20$, 100, and 300 s.
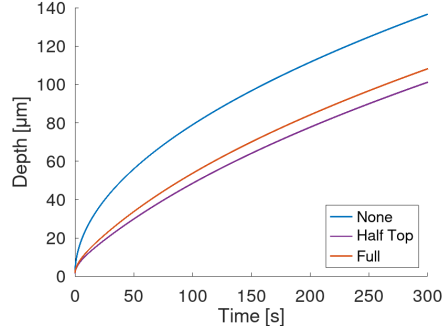
Figure 8: The comparison between depth in time curves depicts faster interface motion when the condition is such that metal ions can leave the interface more easily.
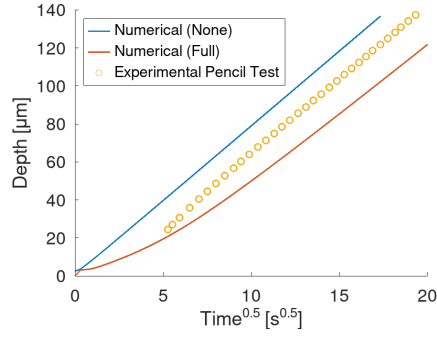

Figure 9: The experimental pencil test depth falls between the numerical depth obtained from using the 'None' and the 'Full' condition.
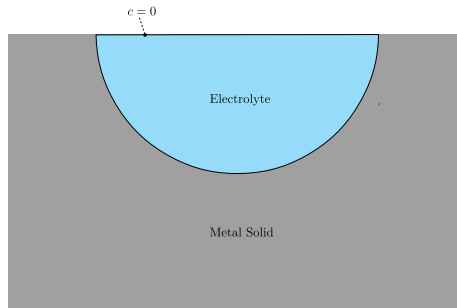

Figure 10: The schematic view of the two-dimensional pit test.

Table 2: Values of the parameters used in the simulations of the two-dimensional pit example.

$\delta_{\mathrm{mesh}} \in \{1.0, 2.0, 3.0, 4.0, 5.0\}\ \mu\mathrm{m}$
$\delta_{\mathrm{time-step}} \in \{0.01, 0.1, 1.0\}\ \mathrm{s}$
$c_{\mathrm{I \to E}} \in \{0.0, c_{\mathrm{sat}}/2, c_{\mathrm{sat}}, 2 * c_{\mathrm{sat}}\}\ \mathrm{mol/mm^3}$
initial pit shape* $\in \{\mathrm{Ci}, \mathrm{Tr}, \mathrm{Re}, \mathrm{Te}\}$

* The shapes are illustrated in Figure 14.

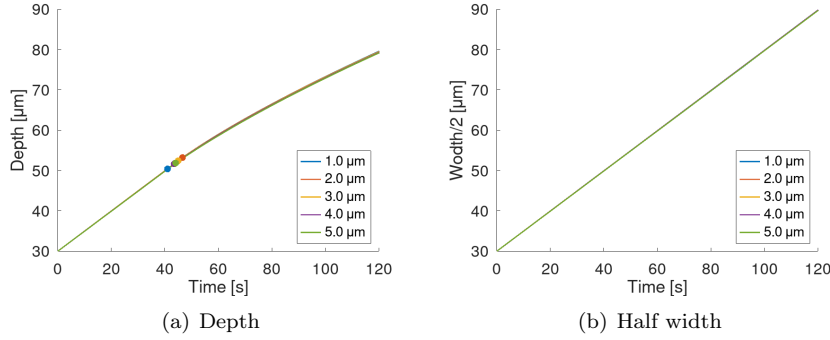(a) Depth   (b) Half width

Figure 11: The curves of a) depth and b) half width of the pit in time for different mesh sizes. The colored points on the depth curve indicate the first time at which the first point on the interface goes to diffusion control condition.

maximum width of the corrosion pit during pit growth. In the simulations, the influence of four parameters on the SRQs are assessed: mesh size, time step size, front-to-electrolyte concentration $c_{\mathrm{I \to E}}$ (which will be described in more detail later), and initial pit shape. The values of these parameters in the simulations are listed in Table 2.

First, a mesh sensitivity analysis has been performed for all values of mesh size in Table 2, $\delta_{\mathrm{time-step}} = 0.1$ s, $c_{\mathrm{I \to E}} = c_{\mathrm{sat}}$, and a semi-circular initial pit shape. Figure 11 shows the depth as well as half width of the pit in time for different mesh sizes. The curves indicate objectivity with respect to the mesh size.

Then, the sensitivity of SRQs of interest are checked against all values of time step size in Table 2, $\delta_{\mathrm{mesh}} = 2.0\ \mu\mathrm{m}$, $c_{\mathrm{I \to E}} = c_{\mathrm{sat}}$, and a semi-circular initial pit shape. Depth and half width results are drawn versus time in Figure 12. The colored points on the depth curve show that the smaller the time step size, the earlier diffusion control occurs, and consequently the slower the interface grows. The figure shows only a negligible time step size sensitivity.

Since a level-set method is utilized to model the motion of the interface, the finite element mesh is fixed during simulations. Consequently, when the interface is moved to its new position at the end of each numerical time increment, a number of finite element nodes on the interface and in the metal solid domain close to the interface fall into the electrolyte domain. Hence, the initial metal ion concentration of these nodes at the start of the next numerical time increment must be specified. This concentration, here, is called 'front-to-electrolyte' concentration $c_{\mathrm{I \to E}}$ and takes a prescribed value in the model. Regarding the fact that the front-to-electrolyte concentration is a model parameter which, to
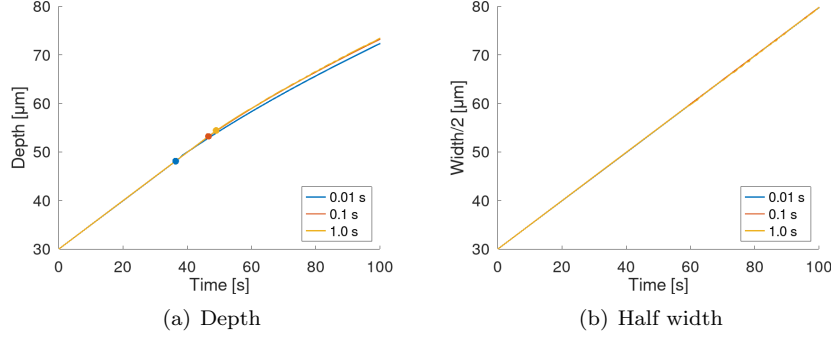
Figure 12: The curves of a) depth and b) half width of the pit in time for different time step sizes. The colored points on the depth curve indicate the first time at which the first point on the interface goes to diffusion control condition.
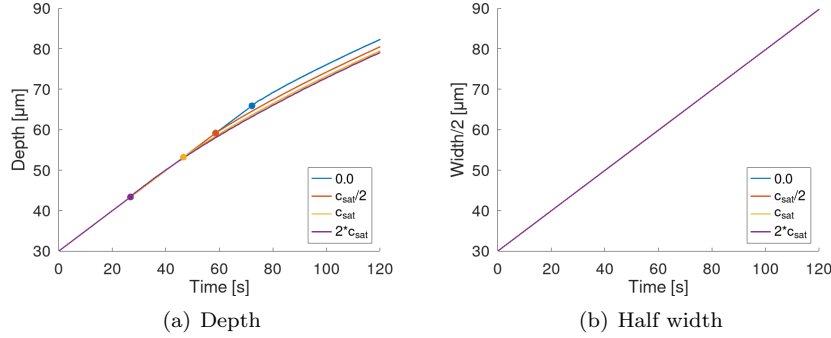

Figure 13: The curves of a) depth and b) half width of the pit in time for different front-to-electrolyte concentrations. The colored points on the depth curve indicate the first time at which the first point on the interface goes to diffusion control condition.

the best of the authors' knowledge, cannot be determined from experiments in
literature, there is uncertainty in its value. To quantify this uncertainty, simulations are conducted for four different values of front-to-electrolyte concentration in Table 2, δ_{mesh} = 2.0 μm, $\delta_{\mathrm{time-step}}$ = 0.1 s, and a semi-circular initial pit shape. Figure 13 shows depth and half width curves for different front-to-electrolyte concentrations. The figure evidently demonstrates that the larger the front-to-electrolyte concentration, the earlier the pit faces the first diffusion control condition on its interface. It should be noted here that temporal scale of the example problem is much larger than the fast chemical reaction time of chloride with metal ion. Additionally, the chloride reaction occurs in a narrow band over the interface whose spatial scale is much smaller than that of the example problem. Thus, the differences between depth showed in figure 13 are neglected in the current example and $c_{\mathrm{I\to E}} = c_{\mathrm{sat}}$ is assumed.

In a real corrosion situation, various factors influence initiation of corrosion (e.g. surface roughness, chemical composition of metal and electrolyte, the size and orientation of grains and their boundaries, the shape of impurities or inclusions on the metal surface, etc.) and thus the initial shape of the pit. Therefore,
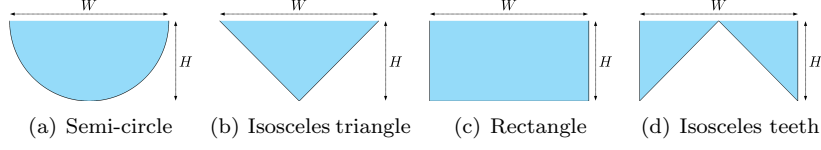
14

Figure 14: Idealized initial shapes of the corrosion pit. (The blue area is the electrolyte domain Ω_{E}, the black line is the interface Γ_{I}, and the solid domain is not shown.)

in the models which assume an initial shape of the corrosion pit, uncertainty quantification of the initial pit shape is necessary. Since there are infinite possibilities of the initial pit shape, only four idealized shapes: semi-circle (Ci), isosceles triangle (Tr), rectangle (Re), and isosceles teeth (Te) are assessed in this paper (see Figure 14). The shapes are proposed such that they are distinct enough and more clearly reveal the evolution of the pit in time. To electrochemically make a distinction between the shapes, four factors are considered: a) the maximum pit depth, b) the largest surface of the electrolyte inside the pit connecting to the electrolyte outside the pit, c) the total mass of electrolyte inside the pit, and d) the total surface area of the interface capable of dissolving the solid atoms into the electrolyte. These factors can be represented by four geometrical parameters of the proposed two-dimensional shapes in the same order just given for the factors: a) height H, b) width W, c) surface area A, and d) the interface length P of the pit. In order to fairly compare the results obtained from different initial shapes, dimensions of the shapes should be specified so that they are equivalent in the sense of the proposed geometrical parameters. Here, the semi-circle is assumed as a reference shape and five equivalence criteria (EC) of the shapes are proposed:

$$
\begin{aligned}
EC1: & \quad H = H_{\mathrm{Ci}}, W = W_{\mathrm{Ci}} \\
EC2: & \quad H = H_{\mathrm{Ci}}, A = A_{\mathrm{Ci}} \\
EC3: & \quad W = W_{\mathrm{Ci}}, A = A_{\mathrm{Ci}} \\
EC4: & \quad H = H_{\mathrm{Ci}}, P = P_{\mathrm{Ci}} \\
EC5: & \quad W = W_{\mathrm{Ci}}, P = P_{\mathrm{Ci}}
\end{aligned}
\tag{15}
$$

where H_{Ci}, W_{Ci}, A_{Ci}, and P_{Ci} are height, width, surface area, and interface length of the semi-circular pit shape, respectively. For example, $EC1$ implies height and width of the shapes be equal to height and width of the semi-circle, respectively. Descriptions of the other equivalence criteria are straightforward as $EC1$. In the simulations of uncertainty quantification of initial pit shape, the radius of the semi-circle R is assumed to be 30 μm. Table 3 lists dimensions of the shapes in all simulations related to initial pit shape. Figure (15(a)) to (15(e)) show the evolution of depth and half width of different initial shapes in different equivalence criteria for $\delta_{\mathrm{mesh}} = 2.0$ μm, $\delta_{\mathrm{time-step}} = 0.1$ s, and $c_{\mathrm{I} \to \mathrm{E}} = c_{\mathrm{sat}}$.

To understand the depth and width evolution more clearly, all pit shape evolutions are visualized in time. As a representative, $EC1$ is selected to illustrate metal ion concentration maps of pits in Figure 16.

Several remarks extracted from above observations and based on model formulation are listed in the following:
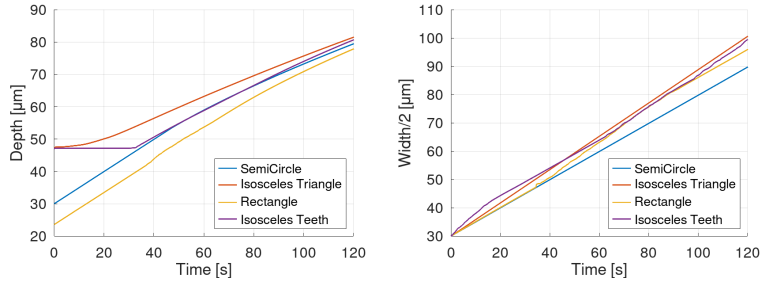
- As being obvious from (6), in activation control condition, the model pre-
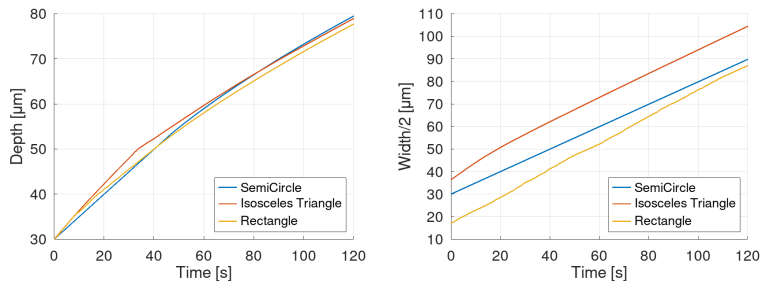
15
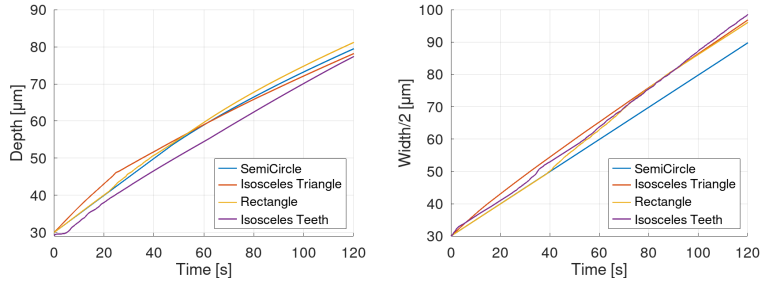
(a) *EC1*

(b) *EC2*

(c) *EC3*

(d) *EC4*

16
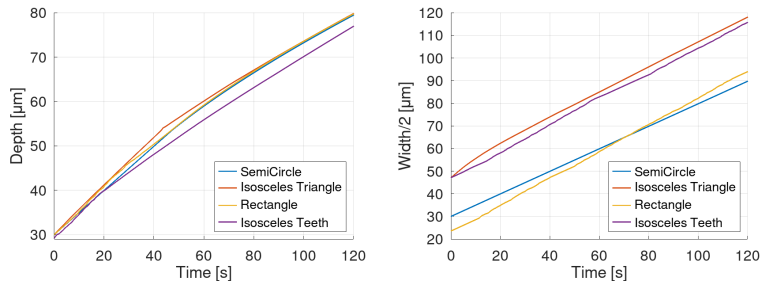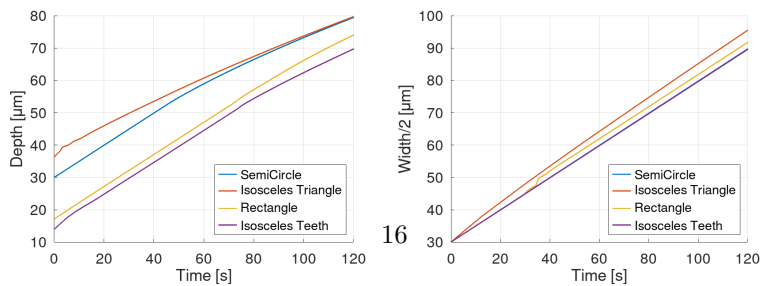
(e) *EC5*

Figure 15: The depth and half width curves of the simulations related to the initial pit shapes according to different equivalence criteria.

(a) $t = 1$ s

(b) $t = 17$ s

(c) $t = 23$ s

(d) $t = 34$ s

(e) $t = 47$ s

(f) $t = 55$ s

(g) $t = 91$ s

(h) $t = 120$ s

Concentration [mol\mm3]

0.0e+00 1e-6   2e-6   3e-6   4e-6   5.1e-06

Figure 16: Metal ion concentration map of pit with different initial shapes according to $EC1$ at selected times.

Table 3: Dimensions of the shapes for different equivalence criteria.
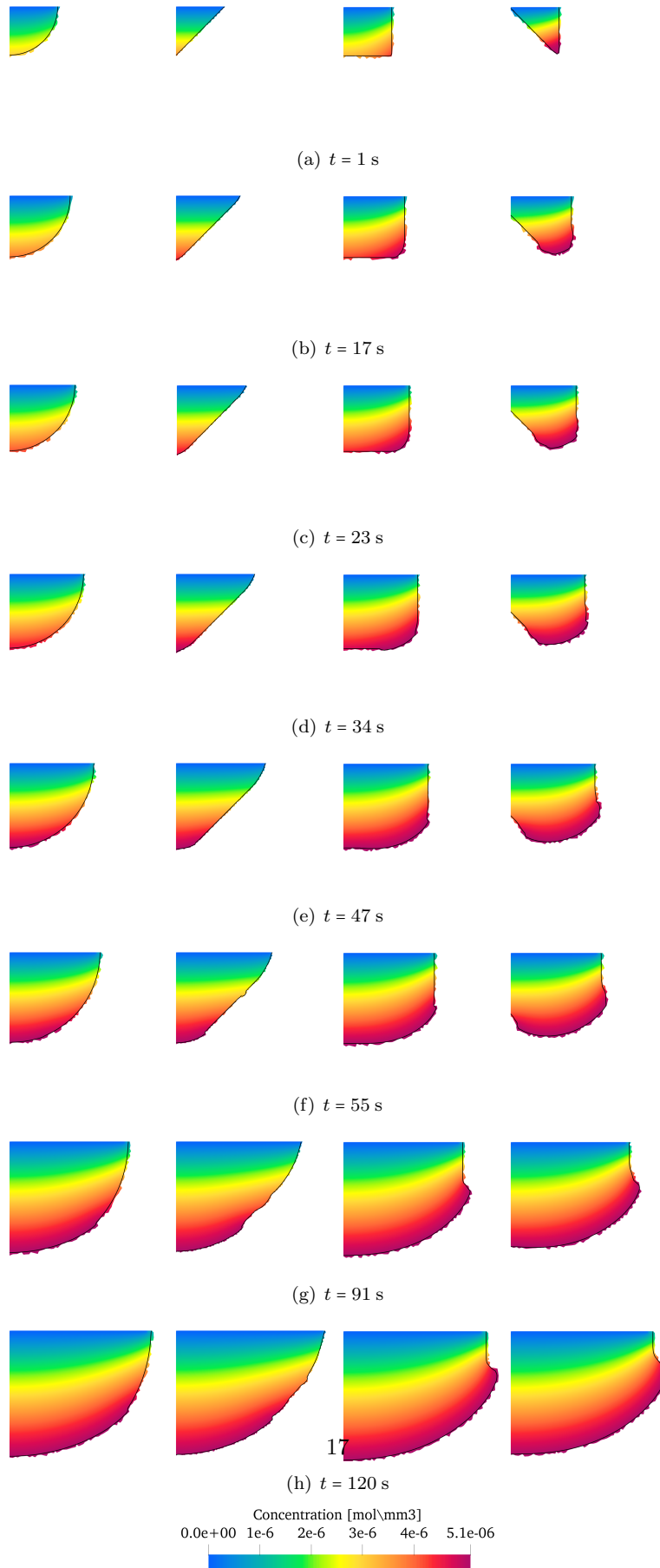
Shape name	Dimensions [μm, μm]	Equivalence criteria				
		$EC1$	$EC2$	$EC3$	$EC4$	$EC5$
Semi-circle	H	30.0	30.0	30.0	30.0	30.0
	W	60.0	60.0	60.0	60.0	60.0
Isosceles triangle	H	30.0	30.0	47.124	30.0	36.341
	W	60.0	94.248	60.0	72.682	60.0
Rectangle	H	30.0	30.0	23.562	30.0	17.124
	W	60.0	47.124	60.0	34.248	60.0
Isosceles teeth	H	30.0	30.0	47.124	*	14.013
	W	60.0	94.248	60.0	*	60.0

* No real-valued height and width can exist for the isosceles teeth shape considering $EC4$. Thus, no simulation case is assigned to it.

dicts the same velocity all over the interface regardless of pit shape. However, at the interface points with a sudden change of slope (i.e. at interface slope discontinuities), the interface velocity is implicitly determined from the vector sum of the interface velocities immediately around these points. That is, the magnitude of interface velocity at these points is larger than interface points around it when having purely anodic dissolution. The interface speed vertices of Triangle is an example of this statement.

- The number of diffusion controlled points on the interface gradually increases from the time of first occurrence of this condition.

- Diffusion control decelerates interface motion as depth increases. In addition, a slope discontinuity (diffusion edge) is initiated on the interface point where diffusion and activation control conditions are competing.

- According to previous remarks, all pit shapes finally tend to a plate shape: a curved shape with a large width and a small height which has an edge at a point between its top and bottom.

- In general, the increase of diffusion controlled interface points in time is directly related to the interface length over surface area ratio in a small local area around the points of the interface. The larger this ratio, the faster the points go to diffusion control.

- For a certain shape, the larger the initial height of a shape, the earlier it encounters diffusion control.

- It seems that a smaller initial width cannot be compensated with other factors such as height, surface area, and interface length except where a diffusion edge appears and evolves.

5.3. Example 3— Four-pits test with interacting corrosion fronts

This example, named 'four-pits', is designed to have the same model properties as the two-dimensional pit example but with the purpose of qualitatively demonstrating capabilities of the model in dealing with noncorrodible and impermeable boundaries as well as merging multiple pits. See the example set-up and metal ion concentration maps in Figure 17 and Figure 18, respectively.
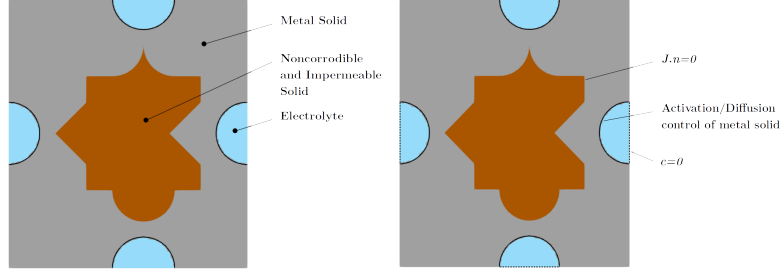
Figure 17: Four-pits example set-up regions, boundary conditions, and dimensions.

The initial metal ion concentration of all pits is assumed to be zero in space. Until 31 s, all pits have the same condition and grow exactly with the same rate. Afterwards, the top, left, and bottom pits face the noncorrodible and impermeable boundary of the middle (brown) solid and automatically divide the metal (gray solid) into three detached parts. The model deals with the noncorrodible and impermeable boundary as well as detachment of metal domain without any special consideration of the level-set method. Then at 49 s, the right pit reaches the middle solid where the metal detaches into five parts and it has diffusion control at the bottom. It is seen at 72 s that the top, left, and bottom pits have evolved to deeper interface points with larger metal ion concentration while the concentration at the right pit's bottom has decreased. A reason for this concentration decrease is the smaller interface length over surface area ratio that locally occurs in the detached metal part in the right v-notch. The mentioned metal part is completely dissolved at 92 s. The top, right, and bottom pits are merged at 109 s, which has been automatically performed by the model without encountering any remeshing issues. At this time, the metal ion concentration at the right bottom of the top and bottom pits has decreased because of a small interface length over surface area ratio. At 123 s all pits have merged. Finally, all metal parts are dissolving with activation control condition at 134 s.

5.4. Example 4— Lacy cover formation

In previous examples, no passivation of the interface is considered. This example involves the activation, diffusion, and passivation control conditions on the interface with the focus on formation of a lacy cover[4] on top of the pit. Figure 19 shows a schematic view of a pit with the lacy cover on its top.

Model parameters are the same as for the two-dimensional pit example except the applied surface electric current density j is equal to 38 mA/mm^2, initial concentration of metal ions in the pit equals to c_{sat}, and a passivation concentration c_{pas} is specified. The formation of lacy cover is composed of three stages: passsivation, reactivation (of passivated parts), and isolation of perforated solid parts. The model incorporates these stages as follows. Finite elements of the interface with at least one integration point with metal ion concentration smaller than or equal to c_{pas} go to the passivation control condition (4) which means no interface motion and metal dissolution at those elements. At the same time, the other finite elements of the interface which are in activation or diffusion control

---

[4]Refer to [26] for the description of the lacy cover formation mechanism.

19

(a) $t = 0$ s   (b) $t = 1$ s   (c) $t = 31$ s

(d) $t = 49$ s   (e) $t = 72$ s   (f) $t = 92$ s

(g) $t = 109$ s   (h) $t = 123$ s   (i) $t = 134$ s

Concentration [mol\mm3]

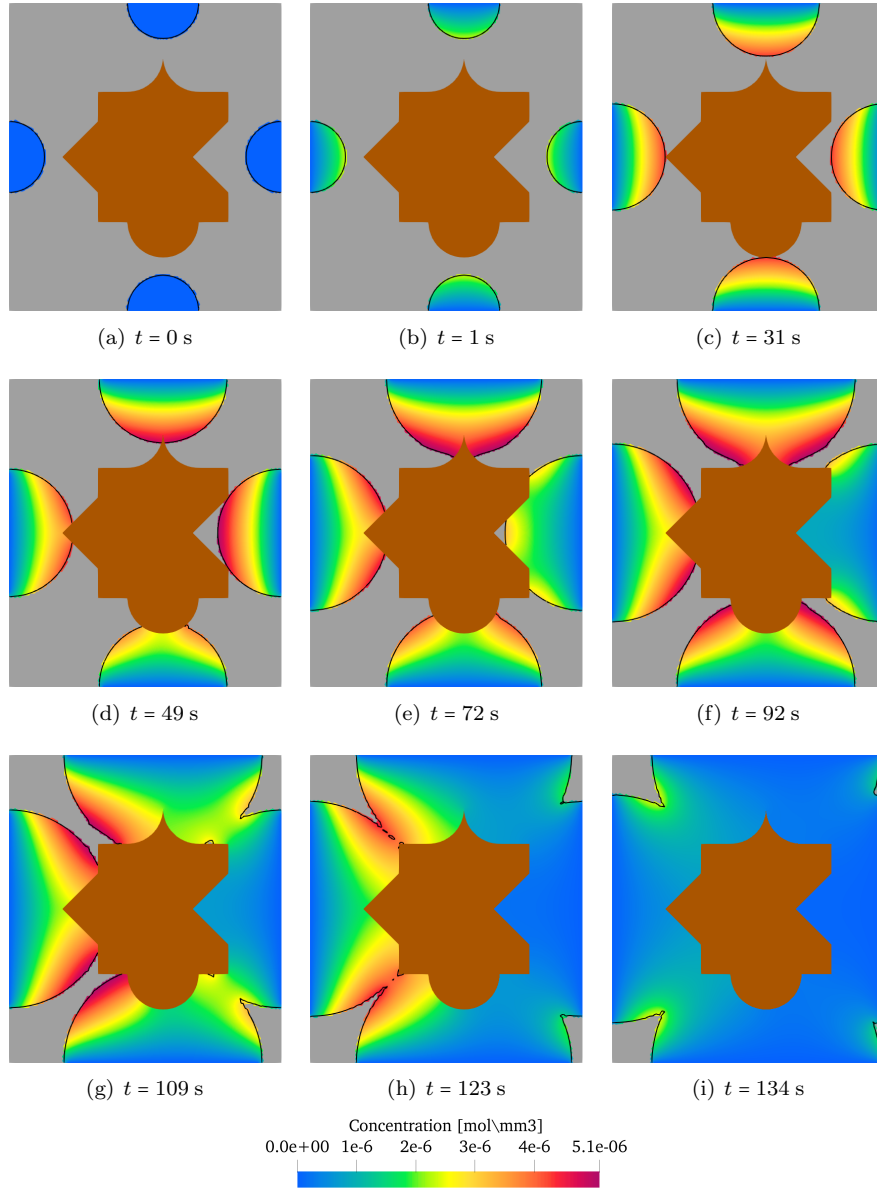0.0e+00   1e-6   2e-6   3e-6   4e-6   5.1e-06

Figure 18: The metal ion concentration map of four-pits example at selected times.
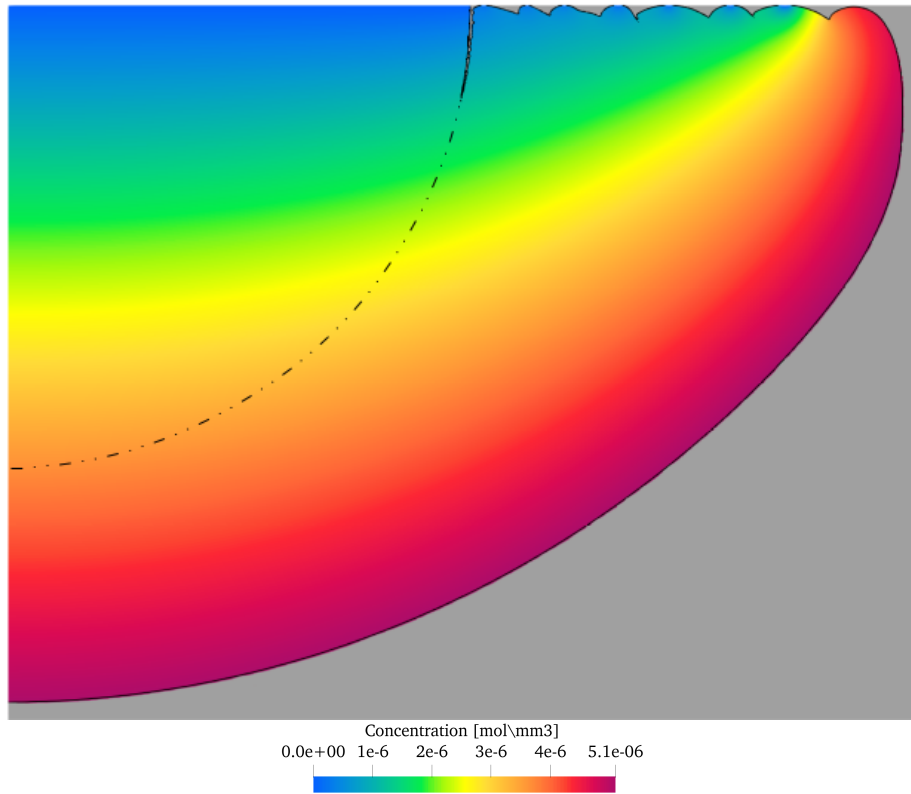
20

Figure 19: Corrosion pit with the lacy cover (i.e. the isolated metal parts) on its top. The gray area is the metal solid domain, the colored area is the metal ion concentration map in the electrolyte domain, the black line is the interface, and the double dot-dashed line is the initial position of the interface.
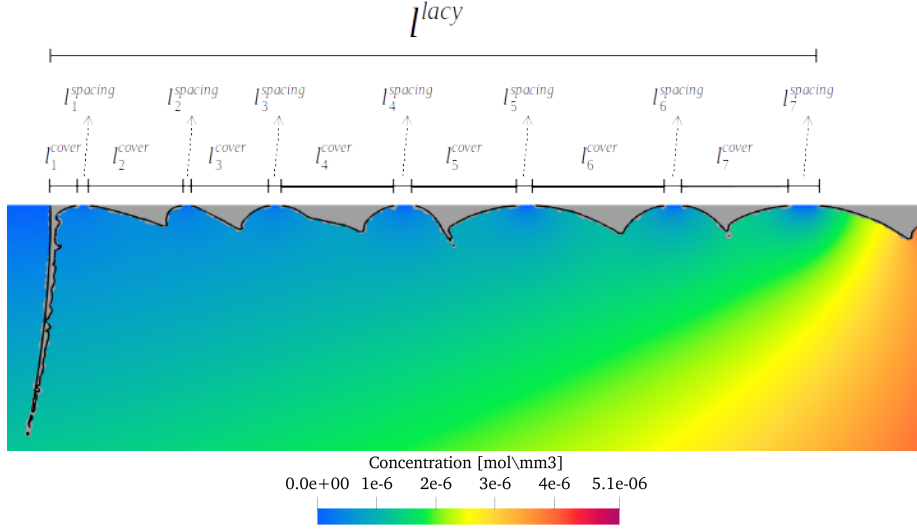
Figure 20: A zoomed view of a lacy cover indicating lacy cover length l^{lacy} and lengths of covers l_i^{cover} and spacings l_i^{spacing}.

condition continue dissolving metal into electrolyte. In addition, the model has a specific criterion for reactivation of the passivated finite elements. Assume a finite element which is active (i.e. in activation or diffusion control condition) is located in the neighborhood of a passivated finite element. It can reactivate the passivated element if the interface progresses into the passivated element. Therefore, passivated finite elements can be reactivated only by their neighbor elements. The competition between passivation and reactivation in the finite elements close to the free surface of electrolyte leads to formation of isolated parts of metal solid on top of the pit which are surrounded by passivated elements. These isolated parts are usually named lacy cover.

The topology of the lacy cover is defined as the system response quantity of interest. Considering the size of a lacy cover with respect to size of the pit and the fact that pit evolution is influenced by the free surface of electrolyte, only the amount of covered parts of the pit top and the spacing between them will be assessed in the lacy cover topology. Assume a lacy cover shown in Figure 20. The total length length of lacy cover l^{lacy} is

$$l^{\text{lacy}} = l^{\text{cover}} + l^{\text{spacing}} \tag{16}$$

where $l^{\text{cover}} = \sum_{i=1}^{n_{\text{lacy}}} l_i^{\text{cover}}$ and $l^{\text{spacing}} = \sum_{i=1}^{n_{\text{lacy}}} l_i^{\text{spacing}}$ are the total length of covers and spacings, respectively, l_i^{cover} and l_i^{spacing} are the length of ith cover and spacing, respectively, and n_{lacy} is the total number of covers or spacings. Dividing equation (16) by l^{lacy} gives

$$1 = \gamma^{\text{cover}} + \gamma^{\text{spacing}} \tag{17}$$

where γ^{cover} and γ^{spacing} are cover length ratio and spacing length ratio, respectively.

Sensitivity analyses of lacy cover topology with respect to finite element mesh size and average time step size are conducted in the points of Figure 21.
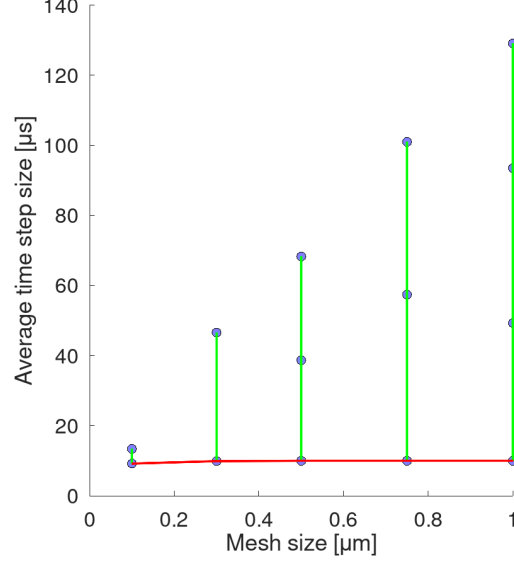
22

Figure 21: The indicated points (blue circles) are used for assessment of lacy cover sensitivity to mesh and average time step size in general. The green lines and the red line are separately checked for time step size and mesh size sensitivity, respectively.

It is worth explaining average time step and the reason for the triangular shaped area containing the points for the sensitivity analysis. In the incremental solution procedure of the model, the Courant-Friedrichs-Lewy (CFL) condition multiplied by a stability factor is used at the end of each time step in order to adapt the time step size of the next step:

$$\delta_{\text{time-step}}^{k+1} = 0.5 \frac{\min\limits_{\Omega} \left(\delta_{\text{mesh}}\right)}{\max\limits_{\Gamma_{\text{I}}} \left(\boldsymbol{v}_{\text{f}}^k \cdot \boldsymbol{n}^k\right)} \tag{18}$$

where $\min_{\Omega}$ is the minimum operator in the whole region of the problem, $\max_{\Gamma_{\text{I}}}$ is the maximum operator along the interface, superscripts $\square^k$ and $\square^{k+1}$ indicate time step k and $k+1$, respectively, and 0.5 is used as the stability factor. Since the incremental solution procedure employs time step adaptation formula (18), time step sizes are scattered in a small range during the each simulation. Thus, the average of these time step sizes are calculated for each sensitivity simulation and shown versus mesh sizes in Figure 21. Moreover, it can be seen from Figure 21 that the average time step sizes are smaller for smaller mesh sizes (i.e. the points shape an almost triangular area), which is in accordance with equation (18).

The sensitivity analysis of lacy cover length ratios are performed with respect to the time step sizes indicated on the green lines of Figure 21. This analysis shows negligible difference between the points on each green line (see Figure 22). That is, the points in each green line are located in an insensitive lacy cover length ratio region. Next, the points on the red line are checked to assess the sensitivity of lacy cover length ratios to mesh size. Figure 23 draws cover length ratio versus mesh sizes of the red line for different values of c_{pas} and c_{sat}. In
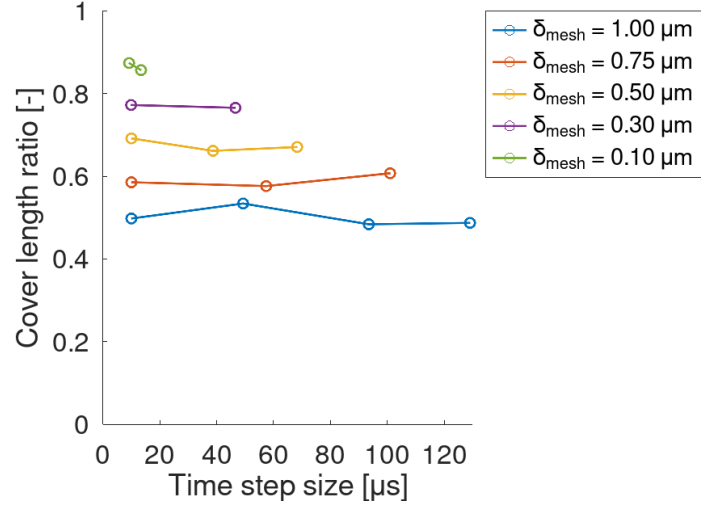
23

Figure 22: The trends of cover length ratio show that the model of lacy cover is insensitive to time step size.
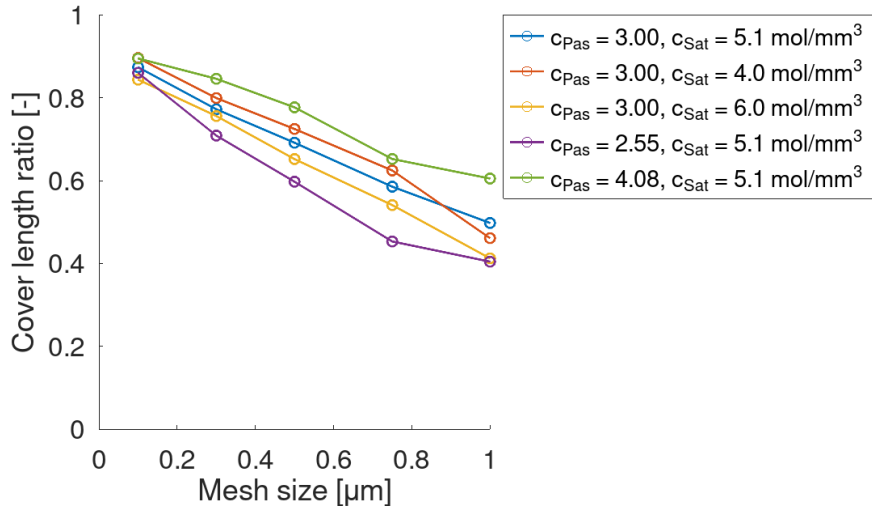

Figure 23: The trends of cover length ratio for different values of c_{pas} and c_{sat} show that the model of lacy cover is sensitive to mesh size.

general, cover length ratio increases with an increase of c_pas and vice versa. This relation is opposite for the c_sat. The only exception is for c_pas = 3.0 mol/mm^3, c_sat = 4.0 mol/mm^3, and δ_mesh = 1.0 μm where cover length ratio is smaller than the case with c_sat = 5.1 mol/mm^3. One reason could be that the lacy length chosen for calculation of lacy cover length ratios does not suffice to obtain a representative value for δ_mesh = 1.0 μm. As obvious from Figure 23, cover length ratio does not approach to a certain value as mesh size is decreased. Hence, lacy cover formation is slightly sensitive to the finite element mesh size.

6. Conclusions

Numerical examples have been designed in Part I to demonstrate the performance of the corrosion model in [15] for pitting corrosion. The model's corrosion interface evolution is not sensitive to the finite element mesh size except in the reactivation process of lacy cover formation. It is also insensitive to time step sizes for all example problems. The model is verified against an analytical solution of a 1D diffusion controlled problem. For this 1D problem, uncertainty quantifications of the extent of initial electrolyte domain and its boundary conditions highlights the importance of accurate determination or assumption of them before simulation. In addition, the experimental validation of depth evolution of two initial electrolyte domain and boundary conditions shows that the experimental depths fall between them, and they can be assumed as upper and lower boundaries of real depths.

There is a parameter in the model which prescribes the concentrations of the finite element nodes which are added to the electrolyte domain as a result of the interface motion into the solid domain. The magnitude of these concentrations depend on spatially and temporally local electrochemical reactions of metal ion with electrolyte. The current corrosion models do not consider such local interactions, and thus uncertainty quantification of this parameter is always required. Prespecification of different values for this parameter shows a slight change in depth over time of a simple 2D corrosion pit.

Because the initiation of the corrosion pit depends on factors such as surface roughness, crystallographic orientations, and inclusions, there is an uncertainty in the initial shape of the pit. Thus, four initial shapes are examined to show the differences in depth and width evolution of a corrosion pit. Overall, it is seen that diffusion control is the main cause of depth and width differences and is reached earlier at deeper points of the interface with higher interface length over surface area ratios. Although the depth and width evolutions of shapes are significantly different, they all finally tend to a plate-like shape when the main part of the interface goes into diffusion control.

The level-set method has provided the model with qualitative properties such as merging multiple pits as well as dealing with sharp noncorrodible and impermeable boundaries without any extra developments. It should be noted that the level-set method does not include computational costs of mesh refinement but adds additional computational effort related to solving the level-set equations.

To simulate formation of a lacy cover on top a corrosion pit, passivation of interface elements is used together with a procedure for reactivation of them. Sensitivity analyses in this paper show that the reactivation procedure is insensitive to time-step size but slightly sensitive to mesh size.

Author Contributions

Amir Fayezioghani: Conceptualization, Methodology, Software, Formal analysis, Writing - Original Draft, Writing - Review & Editing
Richard Dekker: Methodology, Software, Writing - Review & Editing
Bert Sluys: Conceptualization, Supervision, Funding acquisition, Writing - Review & Editing

Acknowledgement

26

References

[1] E. Bardal, Corrosion and Protection, Engineering Materials and Processes, Springer London, London, 2004. `doi:10.1007/b97510`.

[2] V. V. Romanov, Corrosion of metals: methods of investigation, Israel Program for Scientific Translations [available from the U.S. Dept. of Commerce, Clearinghouse for Federal Scientific and Technical Information, Springfield, Va.], Jerusalem SE, 1969.

[3] G. . T. Bakhvalov, A. V. Turkovskaia, Corrosion and Protection of Metals, 1st Edition, MDPI, Oxford SE, 1965.

[4] Y. F. Cheng, Stress Corrosion Cracking of Pipelines, John Wiley and Sons, Inc., Hoboken, NJ, USA, 2013. `doi:10.1002/9781118537022`.

[5] R. J. H. Wanhill, R. T. Byrnes, Stress Corrosion Cracking in Aircraft Structures, in: Aerospace Materials and Material Technologies : Volume 2: Aerospace Material Technologies, Indian Institute of Metals Series 2509-6419 TA - TT -, Singapore : Springer Singapore : Springer, 2017, pp. 387–410. `doi:10.1007/978-981-10-2143-5`.

[6] D. A. Rosario, R. Viswanathan, C. H. Wells, G. J. Licina, Stress Corrosion Cracking of Steam Turbine Rotors, CORROSION 54 (7) (1998) 531–545. `doi:10.5006/1.3284881`.

[7] K. Ali, D. Peng, R. Jones, R. R. Singh, X. L. Zhao, A. J. McMillan, F. Berto, Crack growth in a naturally corroded bridge steel, Fatigue and Fracture of Engineering Materials and Structures 40 (7) (2017) 1117–1127. `doi:10.1111/ffe.12568`.

[8] S. Scheiner, C. Hellmich, Finite Volume model for diffusion- and activation-controlled pitting corrosion of stainless steel, Computer Methods in Applied Mechanics and Engineering 198 (37-40) (2009) 2898–2910. `doi:10.1016/j.cma.2009.04.012`.

[9] S. Silling, Reformulation of elasticity theory for discontinuities and long-range forces, Journal of the Mechanics and Physics of Solids 48 (1) (2000) 175–209. `doi:10.1016/S0022-5096(99)00029-0`.

[10] Z. Chen, F. Bobaru, Peridynamic modeling of pitting corrosion damage, Journal of the Mechanics and Physics of Solids 78 (2015) 352–381. `doi:10.1016/j.jmps.2015.02.015`.

[11] W. Mai, S. Soghrati, R. G. Buchheit, A phase field model for simulating the pitting corrosion, Corrosion Science 110 (2016) 157–166. `doi:10.1016/j.corsci.2016.04.001`.

[12] S. Osher, R. Fedkiw, K. Piechor, Level Set Methods and Dynamic Implicit Surfaces, Applied Mechanics Reviews 57 (3) (2004) B15–B15. `doi:10.1115/1.1760520`.

[13] R. Duddu, Numerical modeling of corrosion pit propagation using the combined extended finite element and level set method, Computational Mechanics 54 (3) (2014) 613–627. `doi:10.1007/s00466-014-1010-8`.

[14] A. S. Vagbharathi, S. Gopalakrishnan, An extended finite-element model coupled with level set method for analysis of growth of corrosion pits in metallic structures, Proceedings of the Royal Society A: Mathematical, Physical and Engineering Sciences 470 (2168). `doi:10.1098/rspa.2014.0001`.

[15] R. Dekker, F. P. der Meer, J. Maljaars, L. J. Sluys, A level set model for stress-dependent corrosion pit propagation, International Journal for Numerical Methods in Engineering 122 (8) (2021) 2057–2074. `doi:10.1002/nme.6614`.

[16] S. Jafarzadeh, Z. Chen, F. Bobaru, Computational modeling of pitting corrosion, Corrosion Reviews 37 (5) (2019) 419–439. `doi:10.1515/corrrev-2019-0049`.

[17] J. S. Newman, K. E. Thomas-Alyea, Electrochemical Systems, 3rd Edition, John Wiley, Hoboken, N.J., 2004.

[18] S. Sharland, A review of the theoretical modelling of crevice and pitting corrosion, Corrosion Science 27 (3) (1987) 289–323. `doi:10.1016/0010-938X(87)90024-2`.

[19] D. Adalsteinsson, J. Sethian, The Fast Construction of Extension Velocities in Level Set Methods, Journal of Computational Physics 148 (1) (1999) 2–22. `doi:10.1006/jcph.1998.6090`.

[20] S. Sarkar, J. E. Warner, W. Aquino, A numerical framework for the modeling of corrosive dissolution, Corrosion Science 65 (2012) 502–511. `doi:10.1016/j.corsci.2012.08.059`.

[21] E. Weinan, Principles of Multiscale Modeling, Cambridge University Press, 2011.

[22] W. L. Oberkampf, C. J. Roy, Verification and Validation in Scientific Computing, Cambridge University Press, 2010. `doi:10.1017/CBO9780511760396`.

[23] P. Ernst, R. C. Newman, Pit growth studies in stainless steel foils. I. Introduction and pit growth kinetics, Corrosion Science 44 (5) (2002) 927–941. `doi:10.1016/S0010-938X(01)00133-0`.

[24] S. Scheiner, C. Hellmich, Stable pitting corrosion of stainless steel as diffusion-controlled dissolution process with a sharp moving electrode boundary, Corrosion Science 49 (2) (2007) 319–346. `doi:10.1016/j.corsci.2006.03.019`.

[25] P. Ernst, R. C. Newman, Pit growth studies in stainless steel foils. II. Effect of temperature, chloride concentration and sulphate addition, Corrosion Science 44 (5) (2002) 943–954. `doi:10.1016/S0010-938X(01)00134-2`.

[26] P. Ernst, N. J. Laycock, M. H. Moayed, R. C. Newman, The mechanism of lacy cover formation in pitting, Corrosion Science 39 (6) (1997) 1133–1136. `doi:10.1016/S0010-938X(97)00043-7`.